High strain rate tensile experiments

Contents

Abstract

A high strain rate tensile testing technique for sheet materials is presented which makes use of a split Hopkinson pressure bar system in conjunction with a load inversion device. With compressive loads applied to its boundaries, the load inversion device introduces tension into a sheet specimen. Detailed finite element analysis of the experimental set-up is performed to validate the design of the load inversion device. It is shown that under the assumption of perfect alignment and slip-free attachment of the specimen, the measured stress-strain curve is free from spurious oscillations at a strain

[4] This Chapter is reproduced from: Dunand, M., G. Gary, and D. Mohr (2013). "Load-Inversion Device for the High Strain Rate Tensile Testing of Sheet Materials with Hopkinson Pressure Bars". *Experimental Mechanics* (In Press). DOI: 10.1007/s11340-013-9712-y.

rate of $1000s^{-1}$. Validation experiments are carried out using tensile specimens, confirming the oscillation-free numerical results in an approximate manner.

3.1 Introduction

The stress-strain response of engineering materials at high strain rates is typically determined based on uniaxial compression experiments on Split Hopkinson Pressure Bar (SHPB) systems (Kolsky, 1949, [96]). In the case of sheet materials, it is difficult to perform a reliable dynamic compression experiment due to limitations associated with buckling. Different techniques have been developed in the past for the high strain rate tensile testing of materials. The key challenges lie in the generation of the tensile loading pulse and the attachment of the specimen to the Hopkinson bars. The specimen gage section is always subject to a tensile pulse, but it is worth differentiating between techniques where the specimen boundaries are subject to tensile loading and those where a compressive loading is applied to the specimen. In the case where the specimen is subject to compressive loading, the loading pulse is inverted within the specimen. When a tensile loading is applied to the specimen boundaries, one may differentiate further between techniques where a tensile loading pulse is generated in the input bar and those where a compressive loading pulse is generated. Throughout our discussion of SHB systems, we will always assume a left-to-right positioning of the specimen, the input bar and the output bar.

Harding et al. (1960, [73]) proposed a technique where the specimen boundaries are subject to tensile loading while a compressive loading pulse is generated in the input bar. They placed a round inertia bar (output bar) inside a hollow tube (input bar). The right specimen shoulder is then connected to the right end of the tube, while the left shoulder is connected to the right end of the inertia bar; both connections are established through mechanical joints (Fig. 3-1a). A rightward travelling compressive loading pulse is generated in the tube which loads the specimen under tension. Only the elastic waves propagating in the output bar are measured in this experiment, therefore requiring two tests with the same loading pulse (one with a specimen, one with the output bar directly connected to the mechanical joint) to measure the force and velocities applied to the specimen boundaries. Nicholas (1981, [135]) and Ellwood et

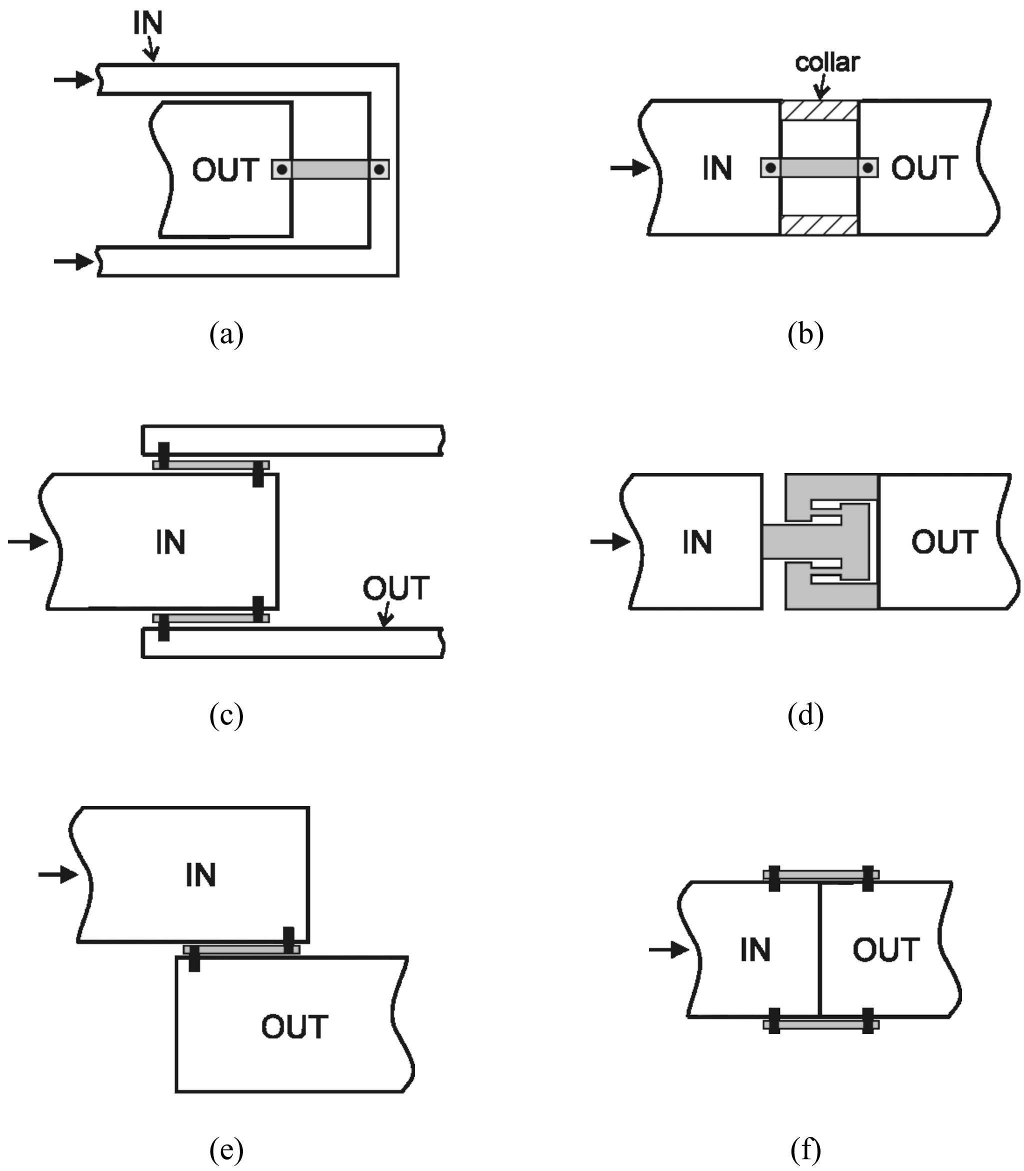

Figure 3-1: Configurations for tensile testing with SHPB systems. The arrows highlight the direction of the incident wave (which is always compression). These schematics just illustrate the basic principle. The black pin-like symbol just indicates the approximate location of specimen attachment and may also correspond to an adhesive or other mechanical joint in reality.

al. (1982, [54]) developed a tensile experiment based on a SHPB system, in which an axisymmetric tension specimen is attached to the bar ends and surrounded by a collar initially in contact with the right end of the input bar and the left end of the output bar (Fig. 3-1b**).** The generated compressive loading pulse is transmitted to the output bar through the collar, without inducing any plastic deformation in the specimen. The loading pulse is then reflected into a tensile pulse at the free right output bar end which then loads the specimen under tension.

As an alternative to inverting the compressive loading pulse within the bars prior to loading the specimen, different techniques have been proposed where the loading pulse is inverted at the specimen level. Lindholm and Yeakley (1968, [112]) developed a hat-shaped specimen (Fig. 3-1c) which is put over the right end of the input bar (input bar diameter equals the hat's inner diameter), while the hat's rim is connected to a tubular output bar that partially overlaps with the input bar (inner output bar diameter equals the hat's outer diameter). Four gage sections are machined in the hat's cylindrical side wall to guarantee a uniaxial stress state at the specimen level. Mohr and Gary (2007, [123]) proposed an M-shaped specimen to transform a compressive loading at the specimen boundaries into tensile loading of the two gage sections (Fig. 3-1d). The M-shaped specimen is used for transverse plane strain tension, which allows shorter gage sections and therefore higher strain rates, and has been validated for strain rates higher than 4,000/s. The key advantage of their technique is that there is no need to attach the specimen to the bars.

For sheet materials, Tanimura and Kuriu (1994, [171]) proposed a non-coaxial SHPB system (Fig. 3-1e). The input and output bars are laterally shifted while a pin joint is used to attach the sheet specimen to the sides of the bars. Mouro et al. (2000, [129]) used a co-axial SHPB system to perform high strain rate tension experiments on sheet metal. They modified the shape of the bar ends such that a two-dimensional multi-gage section hat-shaped sheet specimen can be inserted between the input and output bars of a SHPB system. The specimen must be bent into the hat geometry prior to testing which introduces additional geometric inaccuracies. Haugou at al. (2006, [74]) adopted a configuration where four specimens are bonded to the external part of two threaded sleeves initially in contact and screwed to the input and output bars (Fig. 3-1f**),** thus permitting to use optical strain measurement methods. Similar to the technique proposed by Nicholas (1981, [135]), the compressive incident wave is thus directly transmitted to the output bar, before the reflected tensile pulse loads the specimens. Instead of inverting a compressive loading pulse, a tensile loading pulse may be directly generated in the input bar using a Split Hopkinson Tensile Bar (SHTB) system. Albertini and Montagnani (1974, [3]) and Staab and Gilat (1991, [163]) generated the tensile loading pulse in the input bar by releasing the elastic energy initially stored in a clamped and pre-stressed section of the input bar. The authors report a rising time of about 40µs to 50µs which is significantly larger than that in SHPB experiments; this is due to the time needed to release the clamping of the pre-stressed input bar. The tensile loading pulse can also be generated through a tubular striker surrounding the input bar and impacting an anvil attached to the input bar end (Ogawa, 1984, [139]). This technique is widely used (e.g. Wang et al., 2000, [188]; Huh et al., 2002, [81]; Smerd et al., 2005, [160]; Van Slycken et al., 2007, [182]; Verleysen et al., 2011, [185]; Guzman et al., 2011, [71]; Song et al., 2011, [161]). It can achieve rising times of the loading pulse of 20µs (Li et al., 1993, [109]). The loading pulse duration is often less than 300 µs in case of steel strikers (e.g. Song et al., 2011, [161]; Gerlacht et al., 2011, [65]) because of technological difficulties in supporting the input bar and the distance required for accelerating the striker bar, but longer pulse durations can be reached with polymeric strikers.

Split Hopkinson bar systems are typically used to perform experiments at strain rates in the range of a few hundreds to a few thousands s^{-1}. In classical Hopkinson bar set-ups, the useful measuring time is limited by the length of the bars, imposing a compromise between the minimum achievable strain rate and the maximum achievable strain. Deconvolution techniques accounting for wave dispersion (e.g. Lundberg and Henchoz, 1977, [115]; Zhao and Gary, 1997, [199]; Bussac et al., 2002, [28]) have been developed to extend the available measuring time, allowing for large deformation experiments at intermediate strain rates. Alternative experimental techniques have also been proposed to perform tensile experiments in the intermediate and high range of strain rates, such as high velocity servo-hydraulic testing machines (e.g. Haugou et al., 2004, [75]; Rusinek et al., 2008, [154]) or direct impact methods (e.g. Tanimura et al., 2003, [171]).

Apart from the method used to generate the tensile loading, a specific issue with high strain rate tensile experiments lies in the attachment of the specimen to the testing apparatus. In the specific case of sheet materials, specimens can be either attached through pin connections (e.g. Tanimura and Kuriu, 1994, [171]), glued (e.g. Haugou et al., 2006, [74]), welded (e.g. Quik et al., 1997, [149]) or hold by friction through curvature (Mouro et al., 2000, [129]) or directly applying high lateral pressure (e.g. Huh et al., 2002, [81]). Pin joints lead to high stress concentrations around the pin/specimen interface, non-negligible deformations outside the specimen gage section and oscillations due to the vibration of the specimen shoulders. The use of epoxy adhesives for specimen attachment appears to reduce the oscillations in the measured force histories. However, it is speculated that this is due to the fact that adhesives act as mechanical filters and therefore suppress the oscillations from the measurements even though these are present within the specimen gage section. In particular, further research is needed to evaluate the influence of the visco-elastic behavior of epoxies on the accuracy of force measurements in SHTB experiments. High pressure clamps appear to be the suitable for attaching the specimen if the applied pressure is large enough to avoid slipping of the specimen and if the inertia of the clamp (including possible screws) is either negligible or matches the impedance of the bar.

In standard Hopkinson bars experiments, measurements of elastic waves propagating in the input and output bars with strain gages permit one to derive the history of force and velocity applied by the bars to each boundary of the specimen (Kolsky, 1949, [96]). In the case of tension experiments where specimen shoulders are wider than the gage section (dogbone shape), bar end displacement can only give an approximation of the strain in the gage section, as it does not take into account the deformation of the transition zones between the gage and clamping sections of the specimen. Optical methods are now widely used for a direct measurement of the strain history in the specimen gage section, such as laser beams (Li and Ramesh, 2007, [110]), Moiré techniques (e.g. Verleysen and Degrieck, 2004, [183]) and digital correlation of high speed video images from a single camera (e.g. Tarigopula et al., 2008, [173]) or stereo DIC with two cameras (e.g. Gilat et al., 2009, [66]).

In this chapter, we propose a new experimental technique for the tensile testing of a single sheet specimen in a modified split Hopkinson Pressure Bar apparatus made of one input bar and two output bars. The proposed technique is particularly adapted to the experimental characterization at high strain rate of the onset of fracture of ductile sheet materials, where large strains need to be reached. A Load Inversion Device (LID) is designed to transform the compressive loading imposed by the bars into tensile loading of the specimen, while limiting the development of bending waves in the output bars. Assuming quasi-static equilibrium of the specimen during loading, the applied force is derived from the stress waves propagating in the output bars, while the deformation of the specimen is measured by Digital Image Correlation (DIC) of high speed video images. Detailed finite element simulations of the experimental apparatus are carried out to evaluate the ability of the device to accurately measure the material behavior. The proposed experimental technique is used to investigate the high strain rate deformation and fracture behavior of TRIP780 steel sheets. In addition to uniaxial experiments, tensile tests are performed on notched specimens at strain rates ranging from 200/s to 1,000/s.

3.2 Load inversion device

3.2.1 Design objective and strategy

The goal is to devise an experimental technique for the tensile testing of Advanced High Strength Steel (AHSS) sheets at strain rates of about 10^2-10^3 s^{-1}. It is worth noting that the ultimate tensile strength of these materials can exceed 1GPa with an engineering strain to fracture of 40% or more. In these experiments, two characteristics of the loading pulse are of critical importance: the rise time and the pulse duration. The rise time must be short enough[5] so that the material is deformed at an approximately constant strain rate before the onset of necking. Note that for example for a rise time of 50µs in an experiment at 1000/s, the material is deformed up to 2.5% strain before a constant strain rate is reached. In addition, the pulse duration must be long enough so that the specimen is deformed up to fracture: at a strain rate of 500/s, a pulse duration of 1ms is required to reach an elongation of 50%. As discussed in the

[5] It is noted that the rise time can also be too short. Very short rise times (e.g. less than 10µs) introduce non-negligible oscillations in the loading.

introduction, it is difficult to achieve a short rise time and a long pulse duration with SHTB systems. Here, we will chose a SHPB system to generate the loading pulse, since reasonably short rise times can be obtained, while the pulse duration can be increased with little technological effort by increasing the length of the striker and input bars.

The use of a SHPB system for tensile testing requires the inversion of the pressure loading pulse either at the specimen level or through a special inversion device. Mouro et al. (2000, [129]) employed a hat-shaped specimen to transform the incoming pulse from compression into tension. However, the hat concept for load inversion is only valid if the mechanical system remains symmetric throughout the entire experiment. In case symmetry is lost, the force acting on individual gage sections can no longer be determined from the measurement of the total force. Since the symmetry is typically lost with the onset of necking, hat-shaped specimens are not suitable for studying the post-necking and fracture behavior of materials. We therefore focus on the development of a load inversion device that allows for the use of a single gage section specimen.

For a SHPB system with the left to right order of striker bar, input bar, specimen, and output bar, the basic principle of load inversion is very simple: instead of attaching the input bar to the left specimen shoulder, it is attached to the right shoulder. Similarly, the output bar is attached to the left specimen shoulder (Fig. 3-1e). As a result, the pressure pulse in the input bar causes the tensile loading of the specimen followed by the compressive loading of the output bar. In reality, this configuration requires an eccentricity of input bar, specimen and output bar axes to avoid contact among these elements. Preliminary finite element analysis revealed that the total force acting on the specimen cannot be determined with satisfactory accuracy when bending waves are present in the output bar. A configuration where two output bars are placed symmetrically on each side of the specimen is therefore chosen. For this configuration, bending waves in the output bars are theoretically omitted. Furthermore, the specimen gage section is no longer obstructed by the bars, thereby enabling the high speed video imaging (HSVI) of the specimen gage section throughout testing. The strains and the instant of onset of fracture can thus be determined from digital image correlation.

3.2.2 Proposed design

The load inversion device is designed to be positioned between the input and output bars of a SHPB system to perform dynamic tension tests. The sheet specimen is attached to the load inversion device, while there is no need for attachments between the device and the bars (transmission of compression through flat contact surfaces only). The proposed device is shown in detail in Fig. 3-2. Its two main components are:

(1) A “pusher” (green) which is positioned between the specimen and the input bar. It comprises a cover plate (grey) and eight screws which apply the clamping pressure necessary to hold the specimen. The pusher inverts the incoming compressive pulse into a tensile loading of the specimen. With the clamping plate attached, it features the same cross-sectional area as the 20mm diameter input bar.

(2) A “stirrup” (red) which holds the specimen and transmits the applied force to the output bars. Each leg of the stirrup matches the cross-sectional area of the corresponding output bar. The shape of the transverse section of the stirrup is optimized to minimize its inertia while limiting its bending during loading, in order to reduce perturbations on the measured force. Note that a slot of the thickness of the sheet specimen has been cut into the stirrup instead of using a floating clamp.

A base plate along with a set of linear guides is used as a positioning system to ensure accurate alignment of the pusher and the stirrup. The linear guides are also used to reduce the bending of the pusher. Note that the eccentricity of the specimen with respect to the input bar is the sum of half the pusher thickness and half the stirrup thickness. All parts of the loading device are made of 4140 alloy steel. The linear guides are made of brass, and contacts with steel parts are lubricated with silicon-based grease to limit friction.

The exact dimensions of the tensile specimen are shown in Fig. 3-3a. It features a 15mm long and 5mm wide gage section. The corresponding elastic wave travel time is about 3μs which is sufficiently short to guarantee the quasi-static loading conditions at the specimen level. Note that a duration of 10μs is needed to apply a strain of 1% at a strain rate of 1000/s.

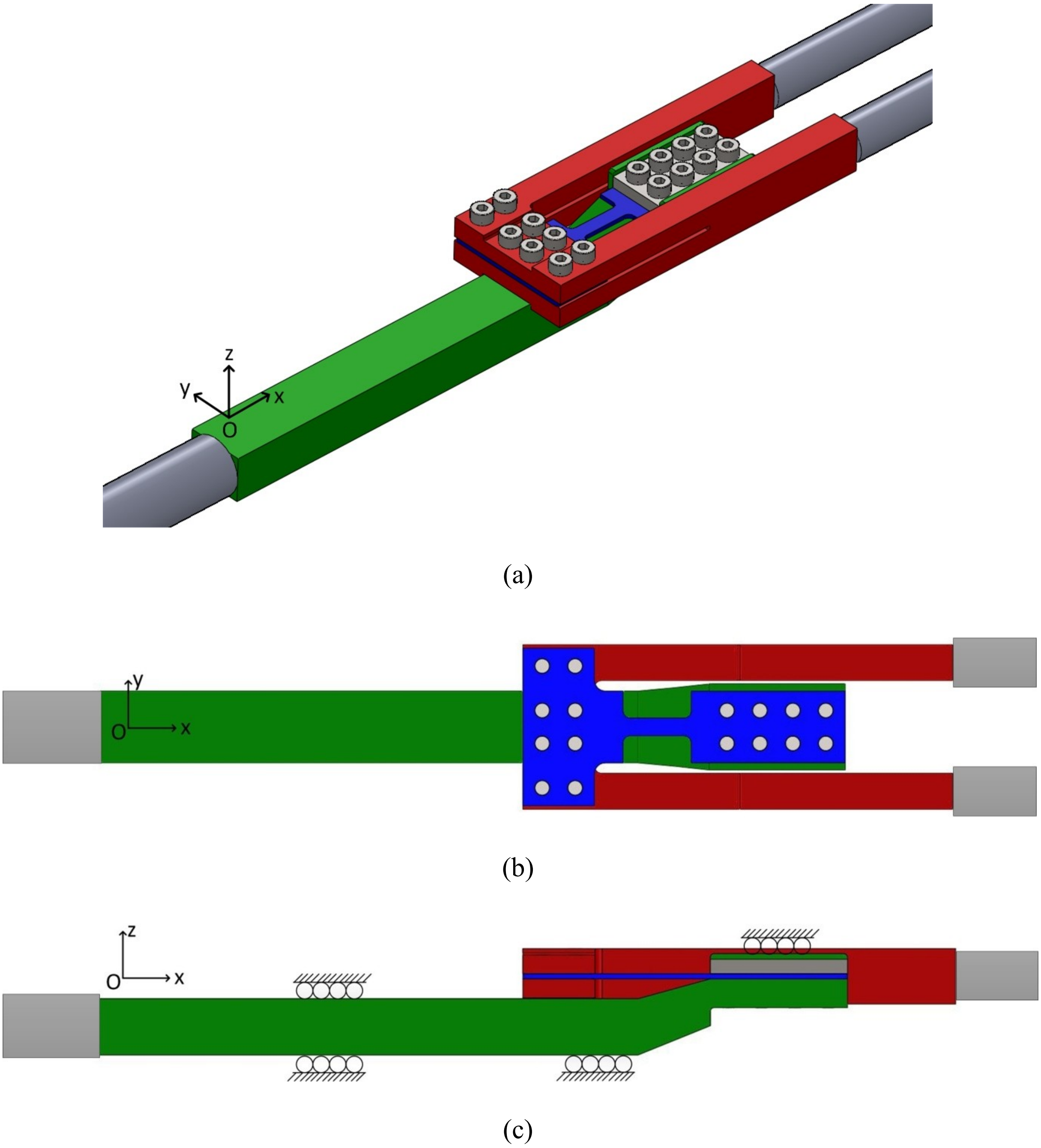

Figure 3-2: Schematic of the Load Inverting Device (LID) including the pusher (green), the stirrup (red) , the specimen (blue) and the input and output bars (grey): (a) isometric view, (b) top view, (c) side view.

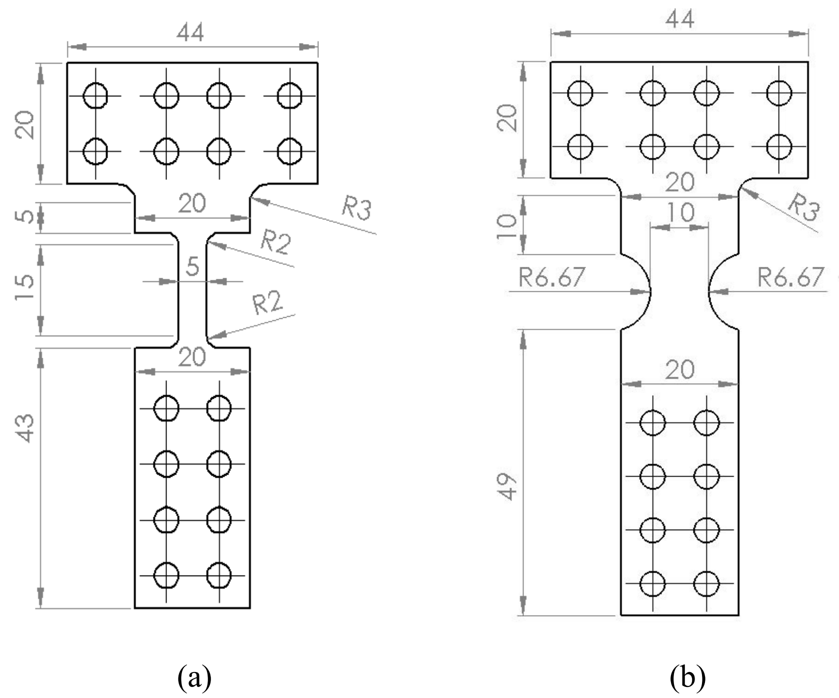

Figure 3-3: Drawings of the specimens for (a) uniaxial tension, and (b) notched tension with cutouts of radius R=6.67mm

3.3 Experimental procedure

3.3.1 Split Hopkinson Pressure Bar (SHPB) system

The SHPB system used in this work consists of the following steel bars:

(1) one 1204*mm* long striker bar of 20*mm* diameter

(2) one 3021*mm* long input bar of 20*mm* diameter; a strain gage is positioned at the center of the input bar;

(3) two 2041*mm* long output bars of 14*mm* diameter; each output bar is equipped with a strain gage positioned at a distance of 299*mm* from the bar-stirrup interface.

As defined by the tensile testing device, the two output bars are positioned at a center-to-center distance of 36*mm*. The rightmost ends of the output bars are attached to a fixed support. This has no effect on the output bar measurements and is only done for initial alignment purposes. It is very important to guarantee an accurate alignment of the output bar ends which are in contact with the stirrup. Note that any misalignment of those surfaces generates spurious waves in the measured output bar signals.

The amplified signal of the strain gages is recorded at a frequency of 1MHz. The recorded strain signals are post-processed with the software package DAVID (Gary, 2005, [64]) to reconstruct the time histories of the axial strain at the end of the input and output bars, following the procedures described in Zhao and Gary (1996, [198]). Low pass filtering, with a cutoff frequency of 100kHz, is used during post processing to remove electrical noise. Accounting for wave dispersion, the measured incident and reflected waves are "transported" to the input bar/loading device interface. Analogously, the measured transmitted waves in the output bars are transported to the output bar/loading device interfaces.

3.3.2 Forces and velocities at the specimen boundaries

The velocities $v_{in}^{LD}(t)$ and $v_{out}^{LD}(t)$ as well as the forces $F_{in}^{LD}(t)$ and $F_{out}^{LD}(t)$ at the boundaries between the SHPB system and the load inversion device are readily given by the formulas (Kolsky, 1949, [96])

$$F_{in}^{LID}(t) = E_{in}A_{in}\left[\varepsilon_{inc}(t) + \varepsilon_{ref}(t)\right] \tag{3-1}$$

$$F_{out}^{LID}(t) = E_{out}A_{out}[\varepsilon_{tra,1}(t) + \varepsilon_{tra,2}(t)] \tag{3-2}$$

and

$$v_{in}^{LID}(t) = -c_{in}\left[\varepsilon_{inc}(t) - \varepsilon_{ref}(t)\right] \tag{3-3}$$

$$v_{out}^{LID}(t) = -c_{out}\varepsilon_{tra,1}(t) = -c_{out}\varepsilon_{tra,2}(t) \tag{3-4}$$

where E is the Young's modulus, A the cross section area, and c the elastic wave velocity. The subscripts "in" and "out" are used to indicate respective reference to the input and output bar properties. $\varepsilon_{inc}(t)$ and $\varepsilon_{ref}(t)$ are the histories of incident and reflected wave at the input bar/pusher interface. $\varepsilon_{tra,1}(t)$ and $\varepsilon_{tra,2}(t)$ are the histories of transmitted wave at the interfaces between the output bars and the stirrup.

The determination of the force and velocity histories at the specimen boundaries requires another "transport" of the signals. Dispersive effects and local structural impedance discontinuities within the LID are neglected because of the short wave travel distances. Assuming an input bar to specimen interface wave travel time of Δt_p, the force at the specimen interface with the pusher is written as

$$F_{in}^{Kolsky}(t) \cong -E_{in}A_{in}\left[\varepsilon_{inc}\left(t-\Delta t_p\right)+\varepsilon_{ref}\left(t+\Delta t_p\right)\right] \tag{3-5}$$

Analogously, denoting time for a wave to travel from the specimen/stirrup interface to the output bar interface as Δt_s, the force at the specimen/stirrup interface reads

$$F_{out}^{Kolsky}(t) \cong -E_{out}A_{out}\sum_{i=1,2}\varepsilon_{tra,i}(t+\Delta t_s) \tag{3-6}$$

It is emphasized that F_{in}^{Kolsky} and F_{out}^{Kolsky} are obtained assuming wave propagation in a slender cylindrical bar. They do not account for possible perturbations of the elastic waves due to geometry or bending of the LID.

Furthermore, we can calculate the corresponding velocities at the specimen boundaries,

$$v_{in}^{Kolsky}(t) \cong -c_{in}\left[\varepsilon_{inc}\left(t-\Delta t_p\right)-\varepsilon_{ref}\left(t+\Delta t_p\right)\right] \tag{3-7}$$

$$v_{out}^{Kolsky}(t) \cong -\frac{c_{out}}{2}\sum_{i=1,2}\varepsilon_{tra,i}(t+\Delta t_s) \tag{3-8}$$

and compute an approximation of the spatial average of the engineering axial strain in the specimen gage section

$$e_{bar}(t) \approx \frac{1}{l_0}\int_0^t [v_{in}(t)-v_{out}(t)]dt \tag{3-9}$$

l_0 is the initial length of the specimen gage section. Note Eq. 3-9 becomes an exact equality if the specimen is perfectly rigid outside the gage section. The wave travel times $\Delta t_p = 41\mu s$ and $\Delta t_s = 28\mu s$ have been determined from finite element analysis. Note that Δt_p is equal to the propagation time of a uniaxial wave in a slender bar of the same length as the pusher.

3.3.3 Local displacement measurements

A high speed video system (Phantom v7.3 with 90mm macro lenses) is employed to record pictures of the specimen surface at a frequency of 111kHz (1 frame every 9µs). A resolution of 448x32 pixels is chosen. The camera is positioned at a distance of about 400mm from the specimen surface, which results in a square pixel edge length of 44µm. A thin layer of white matt paint is applied to the specimen surface along with a black speckle pattern of a speckle size of about 70µm. An exposure time of 1µs is set up with a 150W halogen bulb providing the necessary lighting of the gage section. The video recording is triggered at $t = T_{tr}$ when the input bar strain gage detects the rising edge of the loading pulse.

The virtual extensometer function of the digital image correlation software VIC2D (Correlated Solutions, SC) is used to determine the relative displacement of two points located on the axis of symmetry of the specimen gage section. For this, a quadratic transformation of a 23x23 pixel neighborhood of each point is assumed. Spline-cubic interpolation of the grey values is used to achieve sub-pixel accuracy. The results are reported in terms of the engineering axial strain

$$e_{DIC}(t_{DIC}) = \frac{\Delta u_{DIC}(t_{DIC})}{\Delta x} \tag{3-10}$$

with Δu denoting the relative displacement of two points of an initial spacing $\Delta x = 6.6mm$, corresponding to 150 pixels. The time coordinate is denoted as t_{DIC} to highlight that the DIC measurements need to be synchronized with the time coordinate t of the SHPB system using the relationship $t_{DIC} = t - T_{tr}$.

3.3.4 Determination of the stress-strain curve

The output force history is used to estimate the stress within the specimen. Its measurement accuracy is significantly higher than that of the input force due to the presence of bending waves in the pusher and the uncertainty associated with the calculation of the difference between the incident and reflected waves. Among the strain measures, the local DIC extensometer measurement is selected to eliminate uncertainties associated with the definition of the effective gage length in Eq. 3-9, and with perturbations affecting the reflected wave. The input bar strain gage measurement is thus only used for validation purposes. Denoting the initial cross-sectional area of the specimen as A_0, the engineering stress is formally defined as

$$S(t) = \frac{F_{out}^{Kolsky}(t)}{A_0} \tag{3-11}$$

while the engineering stress-strain curve is obtained from the combination

$$S(e) = [S \circ e_{DIC}^{-1}](e) \tag{3-12}$$

Cubic spline interpolation is used to approximate the strain history between two successive DIC measurements. Note that after the onset of necking (e.g. after reaching the maximum engineering stress), the measured engineering strain must be interpreted as normalized relative displacement. While inverse analysis is needed to determine the stress-strain curve in the post-necking range, the logarithmic axial strain $\varepsilon(t)$ and true axial stress $\sigma(t)$ prior to the onset of necking are given by the well-known relationships

$$\varepsilon(t) = \ln\big(1 + e(t)\big) \tag{3-13}$$

$$\sigma(t) = S(t)[1 + e(t)] \tag{3-14}$$

It is emphasized that the determined stress-strain curve is only valid if the assumption of quasi-static equilibrium is satisfied at the specimen level. This can be verified by comparing the input and output force histories at the specimen boundaries. Due to the poor measurement accuracy of the input force, it is recommended to make use of transient finite element analysis to verify the assumption of quasi-static equilibrium.

3.4 FEA-based validation

The ability of the experimental technique to measure accurately the mechanical specimen response relies on two main hypotheses:

(1) the specimen gage section is loaded under quasi-static equilibrium, and

(2) the loading device, and especially the stirrup, does not significantly perturb the propagation of elastic waves, so that histories of the forces measured in the output bars correspond to the history of force applied to the specimen boundary.

Here, a detailed finite element analysis of a dynamic experiment is performed to assess the validity of these assumptions. As compared to the experimental validation, the FEA approach has the advantage of validating the experimental design independent of possible practical problems associated with the alignment of parts or the clamping of the specimens. Our 3D model of the experimental setup includes the specimen, load inverting device as well as the input and output bars. The striker bar impact is not modeled. Instead, the measured incident wave pulse is directly applied to the free end of the input bar.

3.4.1 Finite element model

The explicit solver of the finite element analysis software Abaqus (2011, [1]) is used to perform the analysis. All parts are meshed with reduced integration 3D solid elements (type C3D8R from the Abaqus element library). The elements of the bar meshes have an edge length of 5mm in the axial direction, and 2mm in the radial direction, allowing for an accurate description of axial frequencies of up to 50 kHz and possible bending waves. The different parts of the loading device are meshed with the same type of elements with an edge length of 1mm. The mesh of the 12mm long and 5mm wide specimen features an edge length of 0.4mm and four elements along the sheet thickness direction. Due to the symmetry of the mechanical system (with respect to the x-y plane defined in Fig. 3-2), only one half of each component is modeled along with the corresponding symmetry boundary conditions. A penalty contact algorithm with a friction coefficient of 0.2 is chosen to model the interaction between the loading device and the bar ends. A tie constraint is defined between the specimen and the LID to represent a slip-free rigid attachment. The specimen material is modeled as isotropic elasto-plastic assuming rate-independent J_2-plasticity. Elements in the gage section are deleted when the equivalent plastic strain reaches a value of 1 at their integration point. All other parts are defined as linear elastic ($E = 210GPa, \nu = 0.3, \rho = 7.82g/cm^3$ for the loading device and the output bars, $E = 185GPa, \nu = 0, \rho = 8.1g/cm^3$ for the input bar). The loading pulse shown in Fig. 4a is applied at the free end of the input bar as surface pressure history. It corresponds to a stress pulse measured experimentally (and transported analytically to the specimen interface) for a striker velocity of 14.8m/s, corresponding to an equivalent plastic strain rate of about 860/s before necking. Note that Poisson ratio of $\nu = 0$ is chosen for the input bar material to avoid geometric dispersion effects on the loading pulse. The numerical simulation is run for 2ms which includes about $630\mu s$ of incident wave travel up to the input bar/pusher interface. A stable time increment of 4.69 10^{-8}s is used by the Abaqus/Explicit solver.

3.4.2 Simulation results

The simulation results include (1) the strain histories at the integration points of elements located at the locations of the input and output bar strain gages (in Fig. 3-4), and (2) the relative displacement of two nodes located on the surface of the specimen gage section (in Fig. 3-5) at an initial distance of 3mm (correspond to the DIC based optical extensometer). The above data processing procedure is applied to these simulation results to determine the stress-strain response of the specimen material. Fig. 3-6a compares the determined true stress versus logarithmic strain curve (solid black line) with the input constitutive behavior (solid red line). The two curves lie almost perfectly on top of each other up to a strain of about 0.25, which confirms the validity of the proposed experimental technique for the determination of the stress-strain response of a typical AHSS sheet material at a strain rate of 900/s. In particular, the assumption that the history of force applied by the specimen to the stirrup is transmitted to the output bars without excessive perturbations is validated through this result. The curves diverge at a strain of 0.25 due to the onset of necking. Beyond this point, the assumption of an approximately uniform strain distribution within the gage section breaks down and the application of Eq. 3-14 is no longer valid. Note that local heterogeneities of the stress and strain fields, inherent to explicit calculations, are sufficient to trigger necking in this simulation as no initial defects were introduced to the mesh.

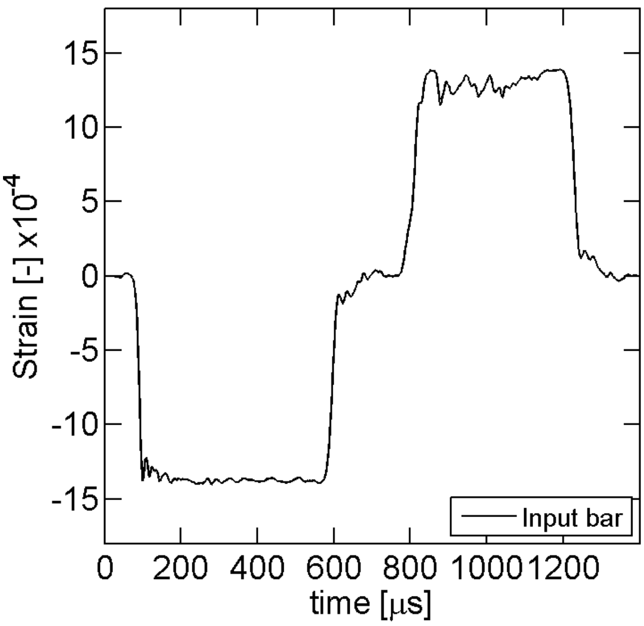

(a)

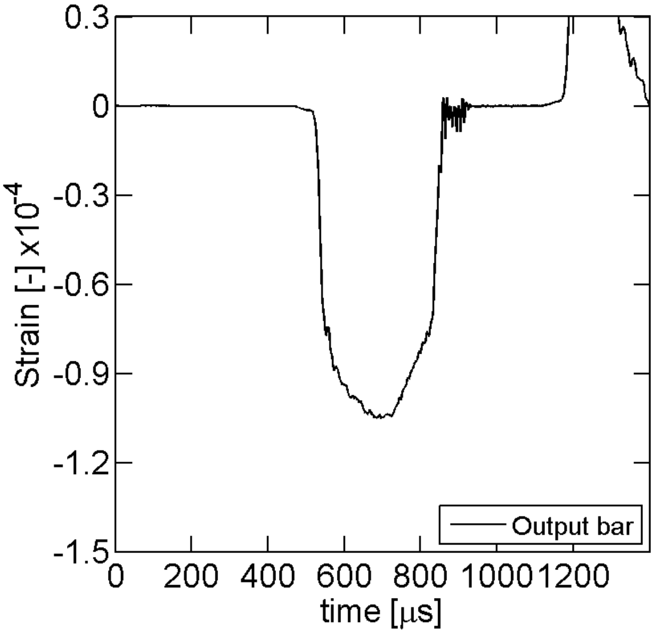

(b)

Figure 3-4: Results from a FE simulation of a uniaxial tension experiment at an average pre-necking equivalent plastic strain of 900/s: signals of (a) the input bar strain gage and (b) the output bar strain gage.

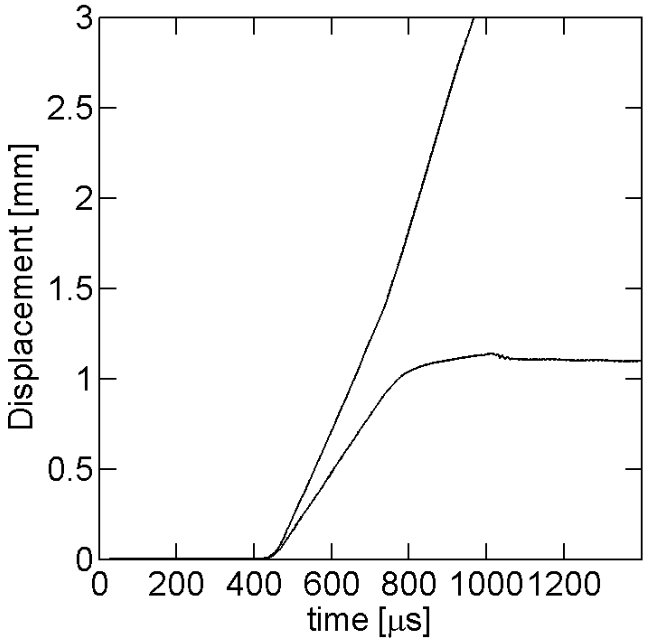

Figure 3-5: Displacement of two nodes located on the surface of the specimen gage section at an initial distance of 3mm, as obtained from a FE simulation of a uniaxial tension experiment at an average pre-necking equivalent plastic strain of 900/s.

To evaluate the assumption of quasi-static equilibrium, we determined the history of the axial forces applied at each boundary of the specimen gage section. The solid curves shown in Fig. 3-6b are obtained by integrating the stress contribution of all integration points located on a cross section of the wide unclamped parts of the specimen. The two curves lie almost perfectly on top of each other, which indicates that the hypothesis of quasi-static equilibrium of the specimen gage section during loading holds true. It is worth noting that despite the short rise time and the omission of pulse shaping, the specimen gage section is in stress equilibrium throughout the entire experiment (except for a very small initial period). The force applied at the stirrup/output bar interface and derived from the transmitted wave measured in the output bar, $F_{out}^{LID,Kolsky}$, is also shown in Fig. 3-6b (as a dashed red line). The force-time signal is delayed by $\tau_{tra} \cong 28\mu s$ which corresponds to the duration associated with the wave travel through the stirrup. However, the amplitude-frequency spectra of both force-time signals are approximately identical, thereby confirming the assumption of negligible axial wave perturbation by the stirrup. On the other hand, the approximation

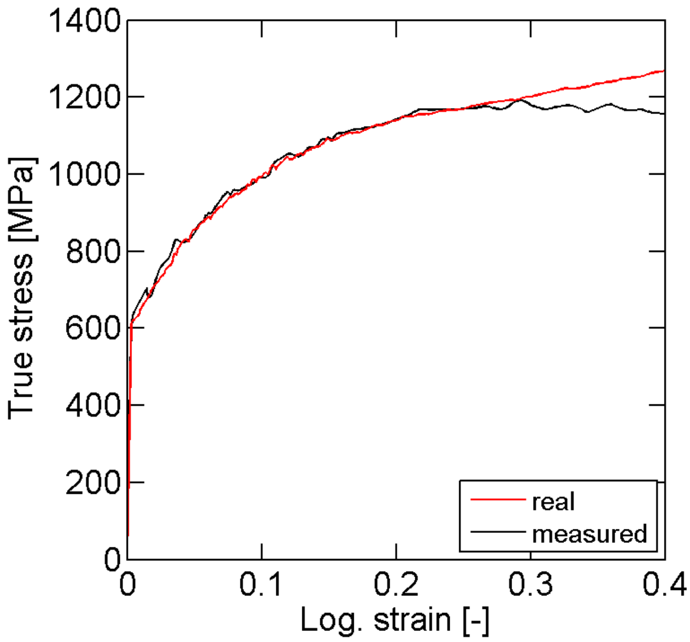

(a)

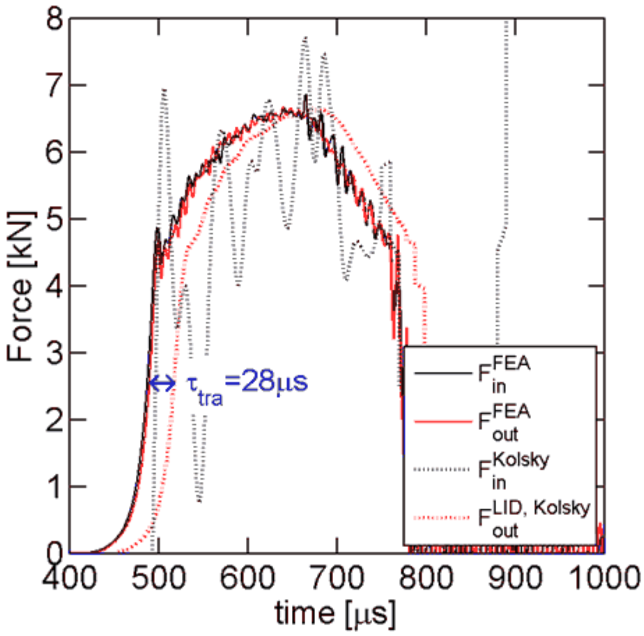

(b)

Figure 3-6: FE-based validation of the experimental technique for uniaxial tension with an equivalent plastic strain rate of about 900/s: (a) Comparison of the stress-strain curve as determined from the virtual measurements (black curve) with the simulation input data (red curve); (b) forces applied at the gage section boundaries by the pusher (solid black line), by the stirrup (solid red curve) and Kolsky approximations, based on elastic waves measured in the bars, of the forces applied at the gage section boundary by the pusher (dashed balck line) and at the output bars/stirrup interface (dashed red line).

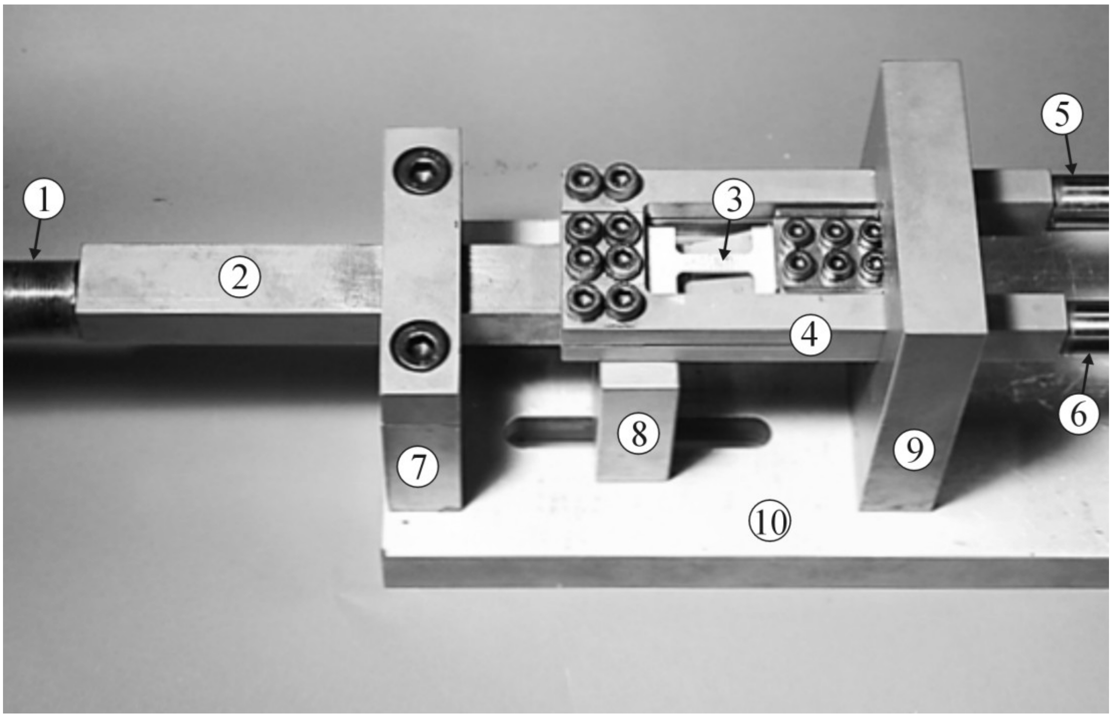

Figure 3-7: Photograph of the load inversion device : (1) input bar, (2) pusher, (3) specimen, (4) stirrup, (5) first output bar, (6) second output bar, (7), (8), (9) guide blocks, and (10) base plate.

of the force applied by the pusher F_{in}^{Kolsky} (dashed black line in Fig. 3-6b), derived from elastic waves measured in the input bar, exhibits strong oscillations compared to the actual applied force F_{in}^{FEA}.Perturbations of the reflected wave due to bending deformation of the pusher have been identified as the major cause of those oscillations, and make the approximation of the applied force measured from the input bar F_{in}^{Kolsky} highly inaccurate.

3.5 Validation experiments

3.5.1 High strain rate uniaxial tension experiments

The uniaxial tension specimens sketched in Fig. 3-3a are extracted from the sheet material through water jet cutting. Within the scope of the present study, the specimen

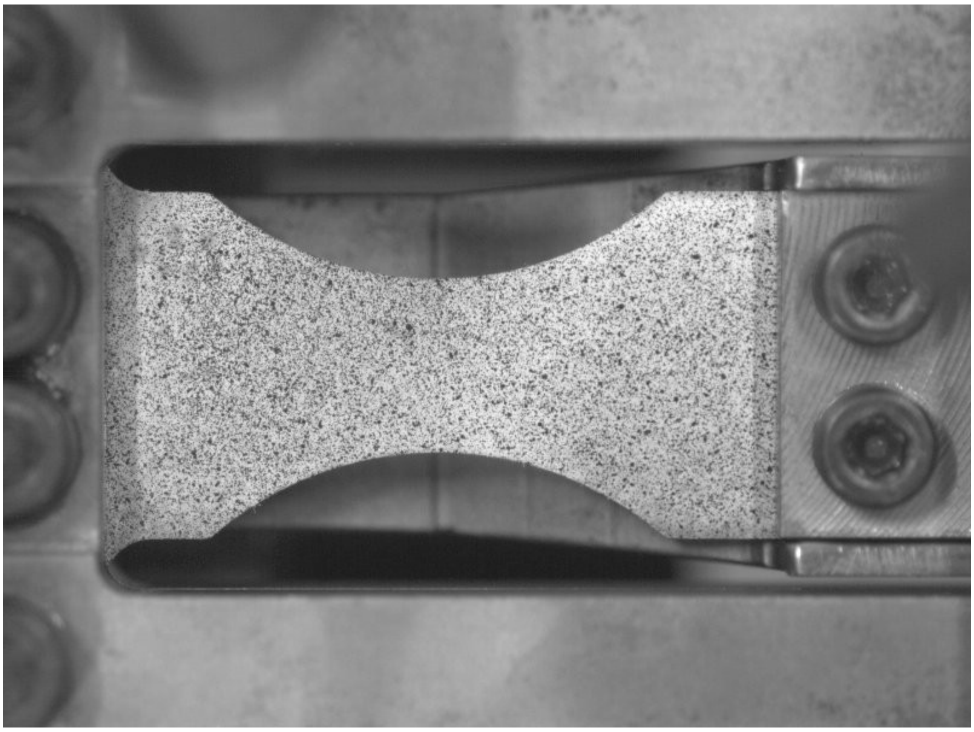

Figure 3-8: Close-up view of a notched specimen positioned in the load inversion device.

loading axis is always aligned with the sheet rolling direction. The dynamic experiments are carried out with striker velocities of 4.2, 11.8 and 14.6 m/s.

Experimental measurements from the test carried out with a striker velocity of 11.8m/s are summarized in Fig. 3-9 to 3-11. The strain history from the input strain gage is shown in Fig. 3-9a while strain histories from output strain gages on both output bars are shown in Fig. 3-9b. Note that the time duration of the recorded reflected wave (Fig. 3-9a) is about $80\mu s$ shorter than the incident wave. After the compressive incident wave pulse is completely transferred into the pusher, contact between the input bar and the pusher is lost. The tail of the tensile reflected wave is thus trapped in the pusher and not recorded by the input strain gage. Before carrying out the test, a static compressive load is applied to the SHPB system. An equal distribution of the load between the two output bars permits to validate the symmetric positioning of the specimen. The two transmitted waves (in Fig. 3-9b) are very close to each other, thereby confirming that the force applied at the specimen/stirrup interface, F_{in}, is split

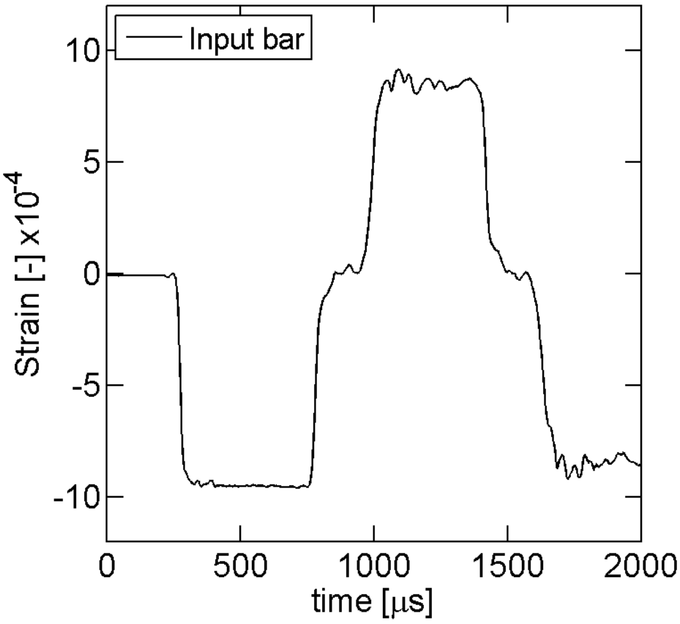

(a)

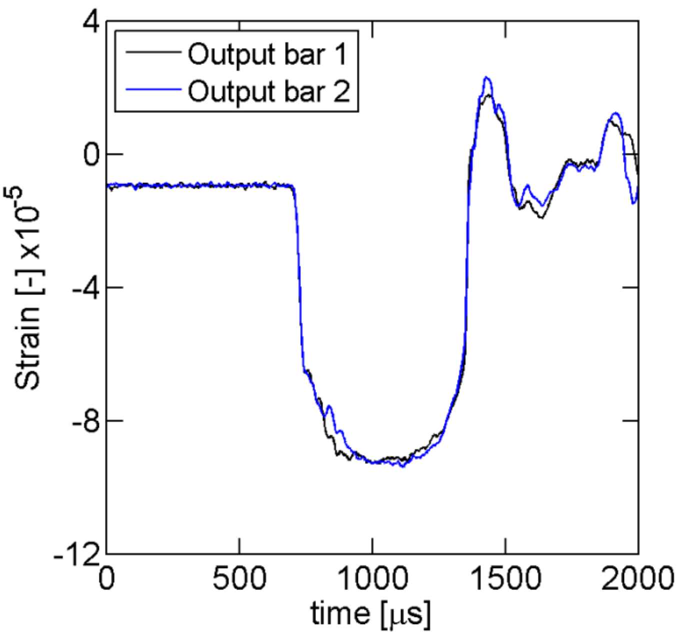

(b)

Figure 3-9: Strain histories of (a) the incident and reflected wave measured from the input bar and (b) the transmitted waves measured from both output bars, during the uniaxial tension experiment with a striker velocity of 11.8m/s.

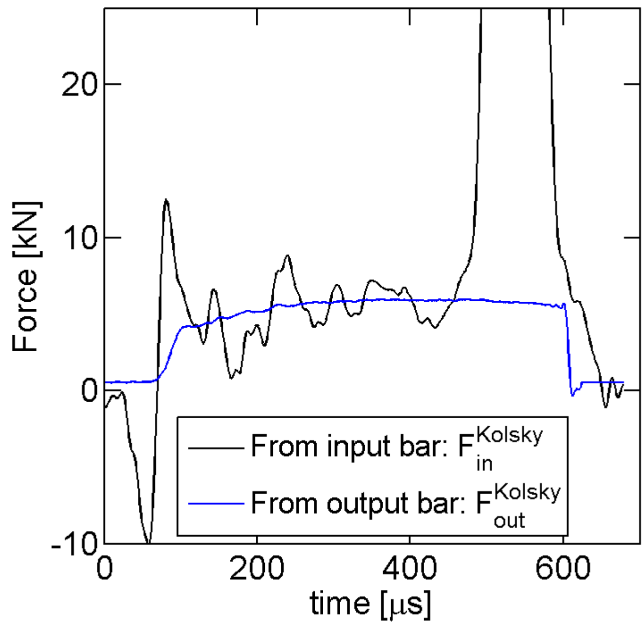

Figure 3-10: Approximation of the forces applied at the specimen/pusher interface , derived from strain waves in the input bar (in black) and at the specimen/stirrup interface, derived from strain waves measured in the output bars (in blue) during the uniaxial tension experiment with a striker velocity of 11.8m/s.

almost symmetrically between both output bars. Small asymmetric perturbations, of less than 3% of the signal in magnitude, can nonetheless be observed. The forces applied at the specimen/pusher interface, F_{in}^{Kolsky}, and the specimen/stirrup interface, F_{out}^{Kolsky}, as derived from strain wave measurements through Eqs. (3-5) and (3-6), are depicted in Fig. 3-10**.** Recall that F_{out}^{Kolsky} is obtained by summing the forces measured in each output bar. The output force F_{out}^{Kolsky} (in blue in Fig. 3-10) exhibits almost no oscillations. On the contrary, the input force F_{in}^{Kolsky} (in black in Fig. 3-10) shows very large oscillations, of the order of the force itself. Beyond those oscillations, both forces have the same magnitude. The oscillations are due to perturbations of the reflected wave created by bending deformations of the pusher during loading. In addition, the input force F_{in}^{Kolsky} largely overestimates the applied force in the last stages of loading because the tail of the reflected wave is trapped in the pusher and not recorded by the strain gage. Therefore, the force obtained from wave measurements in the input bar, F_{in}^{Kolsky}, does not represent accurately the force applied at the specimen/pusher inter-

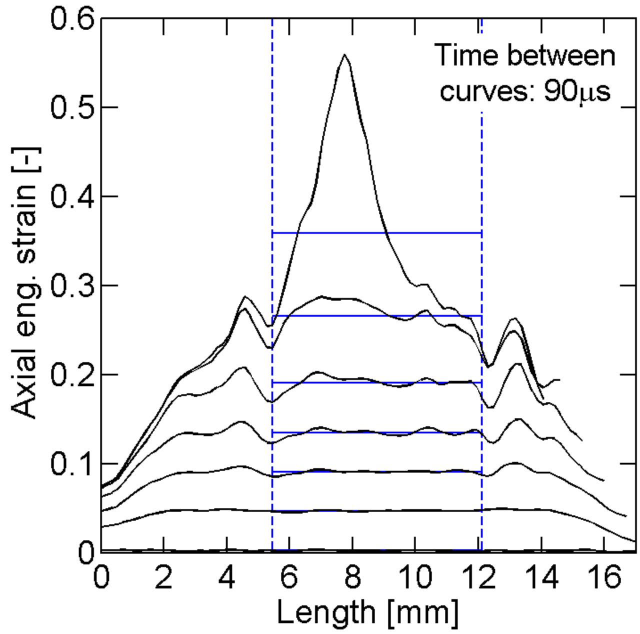

Figure 3-11: Axial engineering strain distribution along the specimen gage section (black solid lines) at different moments in time, as measured by DIC in the uniaxial tension experiment with a striker velocity of 11.8m/s. A time interval of $90\mu s$ is taken between two consecutive curves. The average engineering strain (defined by Eq. 10) is shown with blue solid lines, and the initial position of the optical extensometer is depicted with blue dashed lines.

face, as already shown by the FE simulation results presented in Section 3.4.2. Note that knowing accurately the output force only is sufficient to get the force applied to the specimen, since equilibrium of the specimen gage section has been verified numerically for strain rates of 900/s. The strain distribution along the specimen axis is shown by black lines in Fig. 3-11 at different moments in time. The initial position of the optical extensometer used to measure the engineering strain of the gage section in Eq. (3-11) is depicted with dashed blue lines, while the average engineering strain corresponding to the different strain distributions is shown by solid blue lines in Fig. 3-11. For strains lower than 0.2, the local strain is approximately uniform inside the optical extensometer, with relative variations to the average engineering strain of less than 5%. The DIC also shows that for strains higher than 0.2, the strains begin to localize at the gage section center, which corresponds to the onset of necking. It is also worth noting

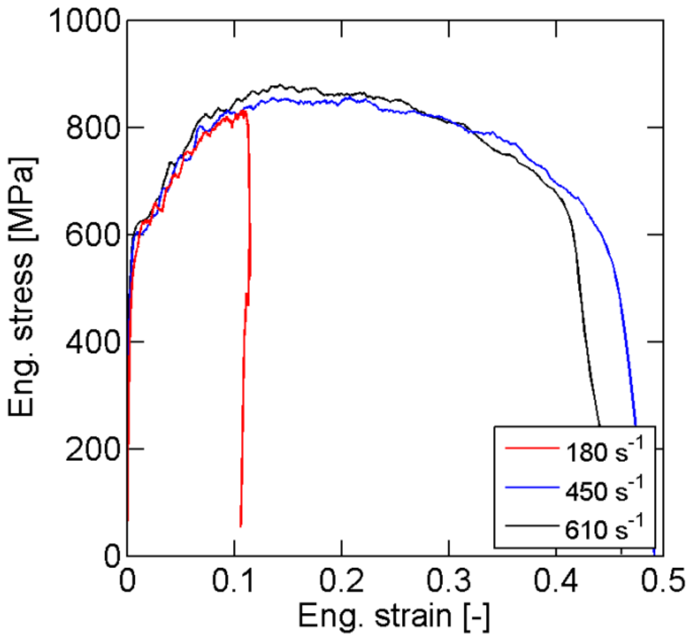

(a)

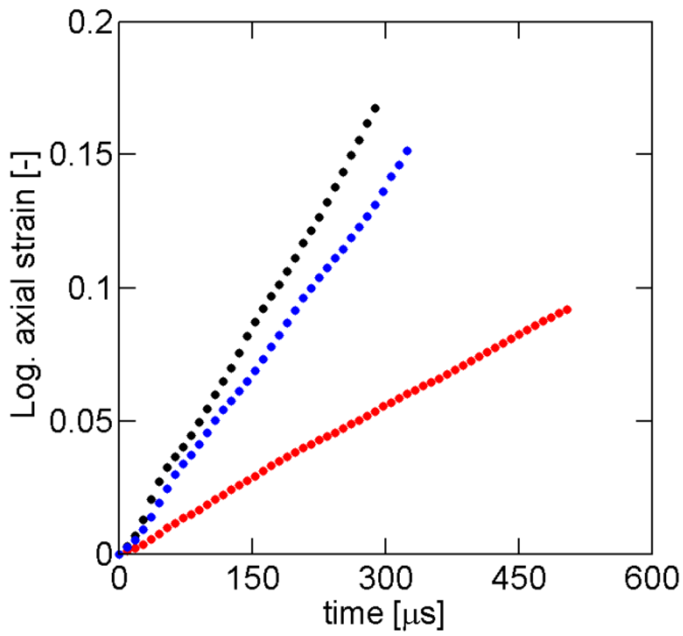

(b)

Figure 3-12: Summary of experimental results for different equivalent plastic strain rates. (a) engineering stress-strain curves. (b) Logarithmic axial strain histories up to the onset of necking (DIC measurements).The time origin corresponds to the first instant when a non-zero strain is measured.

that two local maxima of strain also appear on each side of the gage section. It is speculated that these are due to geometric imperfections of the specimen.

The experimental results for the different striker velocities, as determined through the above experimental procedure, are summarized in Fig. 3-12. The history of the DIC based logarithmic axial strain before the onset of necking is shown in Fig. 3-12b. After about 1% strain corresponding to the rise time of the loading pulse, all strain histories have an approximately constant slope which defines the average pre-necking strain rate. The respective average pre-necking strain rates for the present experiments are 180/s, 450/s and 610/s. The corresponding engineering stress-strain curves are shown in Fig. 3-12a. The same 1200mm long striker bar is used for all experiments resulting in a loading pulse duration of about 550μs. Except for the experiment at 185/s, this duration is long enough to deform the specimens all the way to failure. The onset of necking (characterized by the force maximum) is observed at an engineering strain of about 0.16 for all experiments. The three curves lie approximately on top of each other, indicating that the material exhibits no noticeable effect of strain rate on the flow stress and strain hardening for the range of high strain rates considered (from 180/s to 610/s). The true stress versus logarithmic strain curve at a strain rate of 610/s is shown up to the point of necking in Fig. 3-13 (solid line). Its comparison with the low strain rate result (dashed line) reveals that for a given strain level, the yield stress is about 100MPa higher in the high strain rate experiments.

The experimentally-measured stress-time signals exhibit small oscillations. Their magnitude appears to be independent of the loading velocity. Oscillations of a magnitude of less than $\pm 10MPa$ are observed for all experiments, corresponding to oscillations of $\pm 75N$ on the force signal measured in the output bars. It is worth noting that the simulated experiment for $900s^{-1}$ (Fig. 3-6b) shows a response with oscillations of about the same magnitude ($\pm 5MPa$). Note that perfect interface conditions (no slip) and perfect alignment of all components are assumed in the simulation. It is therefore concluded that the realization of the high strain rate experiment has been successful from a technical point-of-view, while the remaining small oscillations are attributed to the nature of the mechanical system.

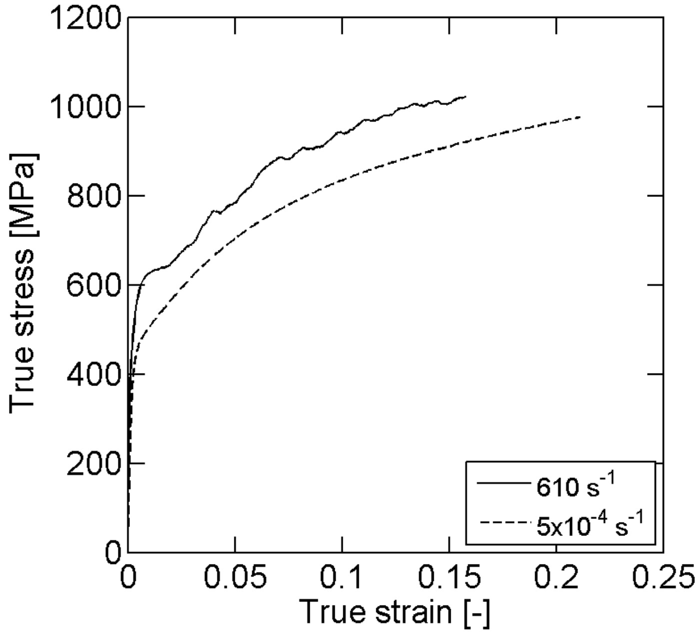

Figure 3-13: True stress-strain curves at pre-necking plastic strain rates of $5x10^{-4}$/s (dashed line) and 610/s (solid line).

3.5.2 Notched tension experiments

The application of the proposed load inversion device is not limited to uniaxial tensile experiments. For illustration, dynamic experiments are performed on notched tensile specimens. These experiments allow for the characterization of the effect of stress state on ductile fracture (see Chapter 4 for details). Here, we perform experiments on specimens with a b=10mm wide notched gage section and notch radii of R=6.67mm (Fig. 3-3b). All tested specimens are cut with their loading axis aligned with the sheet rolling direction. Experiments are performed with striker velocities of 7.1m/s and 10.5m/s. Throughout each experiment, the relative axial displacement between two points on the specimen shoulders is measured using DIC and synchronized with the corresponding axial force history measurements. The initial length of the optical extensometer is $l_0 = 30mm$. The force-displacement curves for high strain rate loading obtained for the $R = 6.67mm$ geometry are shown in Fig. 3-14a (solid lines) next to the curve for low strain rate loadings (dashed line, crosshead velocity of 0.5mm/min. As for the uniaxial tension experiments, the results are almost independent from the striker velocity for the two geometries. However, the force level

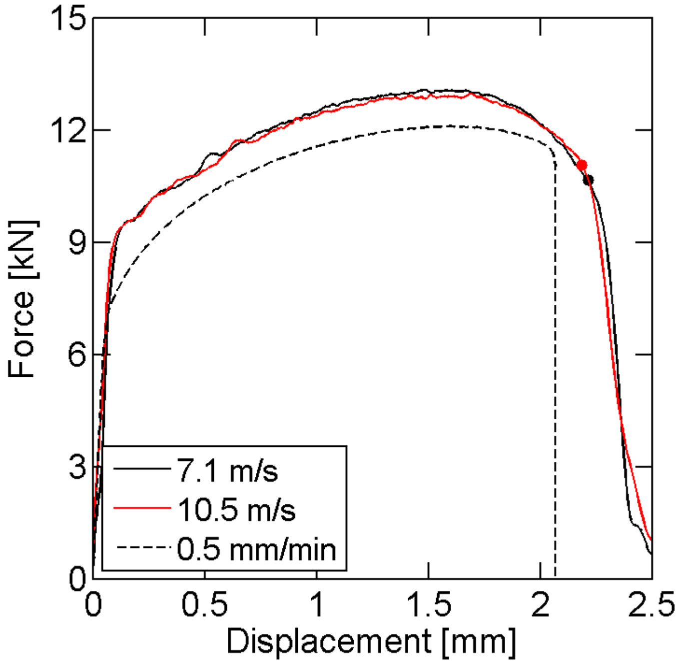

(a)

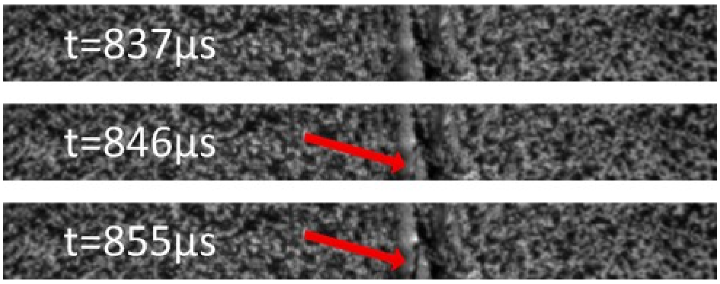

(b)

Figure 3-14: Experiments on a notched tensile specimen. (a) Force-displacement curves for high strain rate loading at different striker velocity (solid lines) and for a low strain rate experiment (dashed line) with a notch radius of *R=6.67mm*. Solid dots depict the instant of the onset of fracture in high strain rate experiments as determined from the occurrence of first surface cracks on (b) high speed photographs taken at a frequency of 110 kHz: the red arrows indicate the location of the first visible surface crack. Note that the time indicated on the pictures is on a shifted time scale.

is about 10% higher than that measured in the low strain rate experiment. The occurrence of a first visible crack on the specimen surface (Fig. 3-14b), corresponding to the onset of material fracture, is highlighted through a solid dot on the measured force-displacement curves. In the case of the slow experiment, a sharp drop in force level is observed at this instant. However, the curves for high strain rate loading exhibit a smooth decrease instead. It is therefore critically important to identify the instant of onset of fracture through high speed photography. The current HSVI system operates at a frequency of 111kHz. Thus, an uncertainty of $\pm 0.05mm$ is associated with the measured displacement to fracture of $2.20mm$.

3.6 Conclusions

A load inversion device is proposed to perform high strain rate tension experiments on sheet materials on conventional split Hopkinson pressure bar (SHPB) systems. The load inversion device includes a pusher which is in contact with the input bar, and a specially designed stirrup which transfers the tensile load in the specimen as compression to two parallel output bars. Two output bars are used to minimize the creation of spurious waves throughout the conversion of the output force from tension to compression. The strains on the specimen surface are measured through planar digital image correlation of high speed video images, while the stresses are computed based on the output bar recordings. As compared to split Hopkinson tensile bar (SHTB) systems, the proposed experimental setup has the technological advantage that the incident wave may be created through a conventional striker-input bar system. The generation of loading pulses with a short rise time and of long duration is therefore easily achieved. These two features are of particular importance when testing sheet materials all the way to fracture at strain rates of only a few hundred s^{-1}.

Detailed finite element simulations are performed to validate the proposed experimental technique. It is shown that for an experimental set-up without any inaccuracies (perfect alignment and gripping of the specimen), the measured stress-strain curve at strain rates of $1000s^{-1}$ would be almost free from oscillations. Validation experiments on specimens extracted from 1.4mm thick TRIP780 steel sheets are also performed which confirm this result in an approximate manner. In addition, experiments are performed on notched tensile specimens to demonstrate the capability of the proposed experimental technique for studying the onset of fracture at high strain rates.